Journal of Engineering Mathematics **42:** 303–319, 2002.

Rapid plunging of a body partly submerged in water

L. LI[1], D.P. PAPADOPOLOUS[1], F.T. SMITH[1] and G.X. WU[2]
Departments of [1]Mathematics and [2]Mechanical Engineering, University College London, Gower Street, London WC1E 6BT, U.K.

Received 1 October 2001; accepted in revised form 20 January 2002

Abstract. The water flow is studied when a thin body, part-submerged in originally still water, is plunged vertically downward. The rapid motion is at medium-to-large Reynolds number. The flow structure consists mainly of two viscous nonlinear layers, namely the unsteady boundary layer on the plunging body and unsteady wake along the trailing free surface, and one inviscid linear region in the bulk of the water. The former produce unsteady displacements which force the motion in the inviscid bulk, along with mixed boundary conditions, and control the evolutions of the wake-side and upper free surfaces. Other regions present are also considered. Analytical and numerical solutions are described, including the effects of the high Froude number and of contact slippage, and the time to bubble formation on the body.

Key words: free surface, nonlinear effects, plunging, semi-submerged, viscous.

1. Introduction

The water motion produced by a plunging body intersecting the water-air surface has been studied under various conditions by [1–8]. This article concerns nonlinear and viscous effects in water flow at medium to high Reynolds numbers Re when a part-submerged body moves by a substantial degree mostly in its own plane. Our motivation came from difficulties encountered in marine-technology and related computations.

The motion of prime concern here is in a two-dimensional vertical plane, with a free surface between water and air, and $\mathrm{Re} \gg 1$. A fundamental problem in that context is for a partly submerged vertical flat plate or thin body being moved in its own plane. Surface-tension effects are omitted in the present study. If gravity is also negligible or its effects are suitably small, then for the case of the vertical plunging flat plate we can expect the major nonlinear motion to occur in thin $O(\mathrm{Re}^{-1/2})$ scaled regions near the plate, specifically in a downward moving unsteady boundary layer attached to the plate and in its unsteady detached wake immediately above which adjoins a trailing free surface (Figure 1). This is because under zero gravity the whole motion is due solely to the downward-moving plate at large Re; without viscous forces there would be no water motion at all in the case of the vertical flat plate.

The contact point, *i.e.* the effective trailing edge where the free surface starts, is assumed at first to not slip relative to the plate; compare [9–14]. Further, the times considered are prior to any water impingement onto the dry plate above that contact point. The aim in this paper is then to determine the induced water flow, the free-surface shapes and criteria on impingement (incipient bubble formation) of the water on to the dry part of the plate.

Sections 2 and 3 describe the flow structure: the nonlinear thin viscous layers near the plate have to be resolved first (Section 2), followed by the linear outer inviscid region (Section 3). Other flow regions generated in this asymptotic treatment of the Navier-Stokes equations are

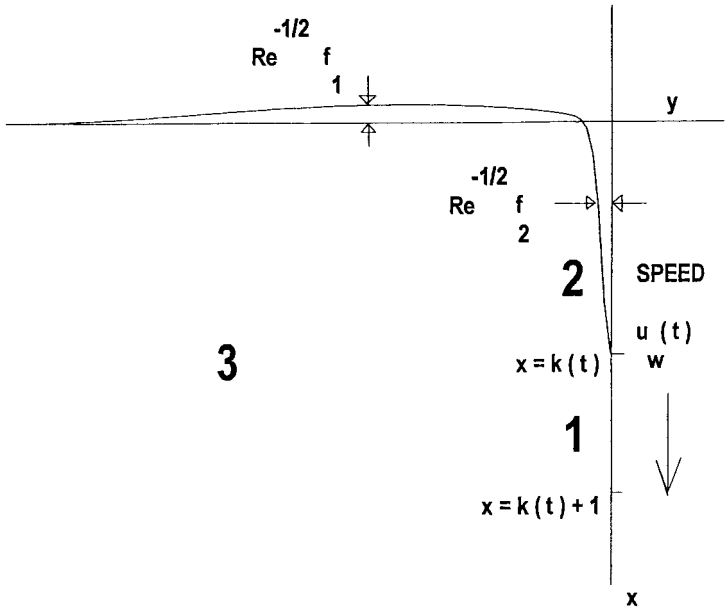

Figure 1. Water-flow regions 1–3 produced by a plunging solid surface (at $y = 0$ in this case).

also considered. Section 4 then presents results for the most basic case of zero gravity and no slip, after which Section 5 examines the influences of Froude number and of slipping at the plate. Attention is drawn to predicted impingement on to the plate surface as the parameters in Sections 4 and 5 are varied. Section 6 gives further comments, on body thickness effects, impingement, the influence of air interaction and allied features.

2. Main viscous regions

The vertical plate is initially at rest in still water. The submerged length L then provides a geometric length scale, which serves to rule out a similarity solution for the complete flow. The plate thereafter moves vertically downward with velocity $u_w(t)$. See Figure 1. Here the vertically downward and horizontally rightward lengths x, y, respectively, are measured in terms of L, while the vertically downward and horizontal velocities u, v and time t are in terms of a representative downward speed U and L/U in turn, the large Reynolds number being $\mathrm{Re} \equiv UL/v$ where v is the kinematic viscosity of the fluid (water); the corresponding stream function is denoted by ψ. If ρ is the constant density, pressure p is measured on ρU^2. The two main regions which have viscous nonlinear flow are the boundary layer region 1 and the wake region 2, with the latter lying at the unknown free surface trailing above the moving contact point. The boundary conditions on the trailing (or side) free surface reduce to $p = 0$, $\partial u/\partial y = 0$ and the kinematic constraint, where the atmospheric pressure is taken as zero. We start here with zero gravity effect (high Froude number, compare with Section 5) and no slip along the plate. Thus, the contact point $x = k(t)$, where $k' \equiv u_w(t)$, remains at the descending trailing edge at a unit distance above the leading edge. Usually we will consider $u_w(t)$ to be unity for all $t > 0$, in which case $k = t$. Outside, the bulk of the fluid remains nearly still in region 3, which is examined in the next section after the discussion of regions 1, 2 below.

The boundary layer lies between the leading edge at $x = k(t) + 1$ and the trailing edge at $x = k(t)$ and has $\partial p/\partial Y$ being negligible, so that p is $o(1)$ to match with the bulk of the slower flow as considered in Section 3 below. It is assumed that $u \sim 1$ and so the classical viscous scalings hold, giving

$$y = \mathrm{Re}^{-1/2}Y, \quad u \sim 1, \quad (\psi, v) = \mathrm{Re}^{-/2}(\Psi, V) \tag{2.1}$$

to leading order, with Ψ zero at the plate. The governing equations are thus

$$u_x + V_Y = 0, u_t + uu_x + Vu_Y = 0 + u_{YY}, \tag{2.2a,b}$$

from the orders of magnitude implied in (2.1) and the property that p is $o(1)$. The boundary conditions are $u = u_w(t)$ and $V = 0$ at $Y = 0$, $u \to 0$ as $Y \to -\infty$, respectively for the no-slip conditions and to match to region 3.

In the wake where $0 < x < k(t)$ the unsteady boundary-layer equations (2.2a,b) again apply, with p small because of the free-surface pressure condition. The equations follow as in (2.1) from a classical argument with V, Ψ of $O(1)$ for the balance of continuity. The side free surface is assumed to be within a normal $O(\mathrm{Re}^{-1/2})$ of the plate at typical $O(1)$ values of x. The y-momentum equation again yields $\partial p/\partial Y$ being negligible, leaving $p(x, t)$ independent of y and hence zero (atmospheric) at leading order. The remaining free-surface conditions require

$$u_Y = 0, -V = f_{2t} + uf_{2x}, \quad \text{at} \quad Y = -f_2(x, t), \tag{2.3a,b}$$

where the unknown side free surface position is $y = -\mathrm{Re}^{-1/2} f_2$, and once again $u \to 0$ as $Y \to -\infty$. However, f_2 can be eliminated from the main problem here by the Prandtl transposition $Y + f_2 \equiv \tilde{Y}$, $V + f_{2t} + uf_{2x} \equiv \tilde{V}$. The governing equations remain (2.2a,b) with $\tilde{V}$, $\tilde{Y}$ replacing V, Y, but the free-surface conditions (2.3a,b) become $u_{\tilde{Y}} = 0$, $\tilde{V} = 0$, at $\tilde{Y} = 0$. We have still $u \to 0$ at large negative $\tilde{Y}$ and we therefore note, for later use, that $\tilde{V} \to -\Psi_x + f_{2t}$ in term of x, Y then.

Moreover, putting $x - k(t) \equiv 1 - \hat{x}$ to measure ($\hat{x}$) upwards from the leading edge, along with the boundary layer's Y (or $\tilde{Y}$ in the wake) $= -\hat{Y}$, $u = 1 - \hat{u}$, V (or $\tilde{V}$ in the wake) $= -\hat{V}$, leaves the governing equations intact yet again but in terms of $(\hat{u}, \hat{V})$ $(\hat{x}, \hat{Y}, t)$ and converts the combined boundary conditions of regions 1, 2 to the form

$$\hat{u} = \hat{V} = 0 \quad \text{at} \quad \hat{Y} = 0 \quad \text{for} \quad 0 < \hat{x} < 1, \tag{2.4a}$$

$$\hat{u}_{\hat{Y}} = \hat{V} = 0 \quad \text{at} \quad \hat{Y} = 0 \quad \text{for} \quad \hat{x} > 1, \tag{2.4b}$$

$$\hat{u} \to 1 \quad \text{as} \quad \hat{Y} \to \infty. \tag{2.4c}$$

We remark that the above is in the case of $u_w = 1$, $k = t$ for $t > 0$. Also the scaled stream function corresponding to $\hat{u}$, $\hat{V}$ is $\hat{\Psi}$ where $\Psi = \hat{\Psi} - \hat{Y}$ for the boundary layer, and in effect f_2 is zero throughout the boundary layer region 1, is nonzero (and assumed positive) throughout the wake portion and is assumed to be continuous and therefore zero at the contact point $\hat{x} = 1$, $x = k$, leaving the horizontal coordinates Y, $\tilde{Y}$, $\hat{Y}$ all zero there. To repeat, the viscous flow solution in regions 1, 2 is unaffected by the side-free-surface shape f_2, except in so far as the Prandtl transposition holds. The major task here is to solve the unsteady boundary-layer equations subject to (2.4a–c).

It follows that we obtain precisely the unsteady boundary-layer and wake problem of an aligned flat plate started impulsively from rest in unbounded fluid. The same reasoning applies to near-vertical bodies of relatively small thickness, while thicker bodies provoke substantial outer inviscid flow which determines the slip velocity at the outer edges of the boundary layer and wake. In the present case the solution for the boundary layer and wake will be described in Section 4 and in particular it gives the scaled unsteady displacement $\delta(x, t)$ as the integral of $(1 - \hat{u})$ over $\hat{Y}$ from 0 to ∞, in the usual way, such that $\hat{\Psi} \sim \hat{Y} - \delta$ and so $\hat{V} \to \partial\delta/\partial\hat{x}$ (which is $-\partial\delta/\partial x$) at large positive $\hat{Y}$, along with $\Psi \to -\delta$ then in the boundary-layer portion (whereas in the wake portion $\partial\Psi/\partial x \to \partial f_2/\partial t - \partial\delta/\partial x$). This displacement effect calculated in Section 4 below drives the outer flow in region 3, as follows.

3. Main inviscid region, and other regions

In the outer flow x, y are of 0(1) and the velocities and pressure are small, say

$$(u, v, \psi, p) = \mathrm{Re}^{-1/2}(u^*, v^*, \psi^*, p^*) \tag{3.1}$$

to leading order. So the nonlinear convection terms and the viscous terms are negligible, leaving the controlling equations

$$u^*_x + v^*_y = 0, \quad u^*_t = -p^*_x, \quad v^*_t = -p^*_y. \tag{3.2a–c}$$

Potential flow thus holds here, controlled by Laplace's equation

$$(\partial^2_x + \partial^2_y)p^* = 0 \tag{3.3}$$

subject to mixed boundary conditions. These are

$$p^* = 0 \text{ at } x = 0 \text{ (along the upper free surface)}, \tag{3.4a}$$

$$p^* \to 0 \text{ at infinity}, \tag{3.4b}$$

$$p^* = 0 \text{ at } y = 0 \text{ for } 0 < x < k, \tag{3.4c}$$

$$p^*_y = -\delta_{xt}(x, t) \text{ at } y = 0 \quad \text{for} \quad k < x < k + 1, \tag{3.4d}$$

$$p^*_y = 0 \text{ at } y = 0 \quad \text{for} \quad x > k + 1. \tag{3.4e}$$

Here (3.4a,c) are free-surface conditions, the upper free surface being assumed to be at $x = \mathrm{Re}^{-1/2} f_1(y, t)$ say (determined below), while the side one is at $y = -\mathrm{Re}^{-1/2} f_2(x, t)$. Condition (3.4b) corresponds to zero motion in the farfield. Condition (3.4d) stems from the boundary-layer region 1, which gives $V = -\hat{V} \to \partial\delta/\partial x$ as $Y \to -\infty$ and hence by matching $v^*_t \to \partial^2\delta/\partial x\partial t$, corresponding to the matching $\psi^* \to -\delta$, and from use of (3.2c). Condition (3.4e) is from the horizontal symmetry below the leading edge.

The potential-flow solution, from Appendix A, yields in particular

$$\Psi_t = -\frac{(\bar{x} - \bar{x}_A)^{1/2}}{\pi} \int_{-\infty}^{\bar{x}_A} \frac{(\bar{x}_A - \bar{\xi})^{-1/2}}{(\bar{x} - \bar{\xi})} [\delta_t(\bar{\xi}, t) - \delta'_0(t)] \, \mathrm{d}\bar{\xi} - \delta'_0(t) \tag{3.5}$$

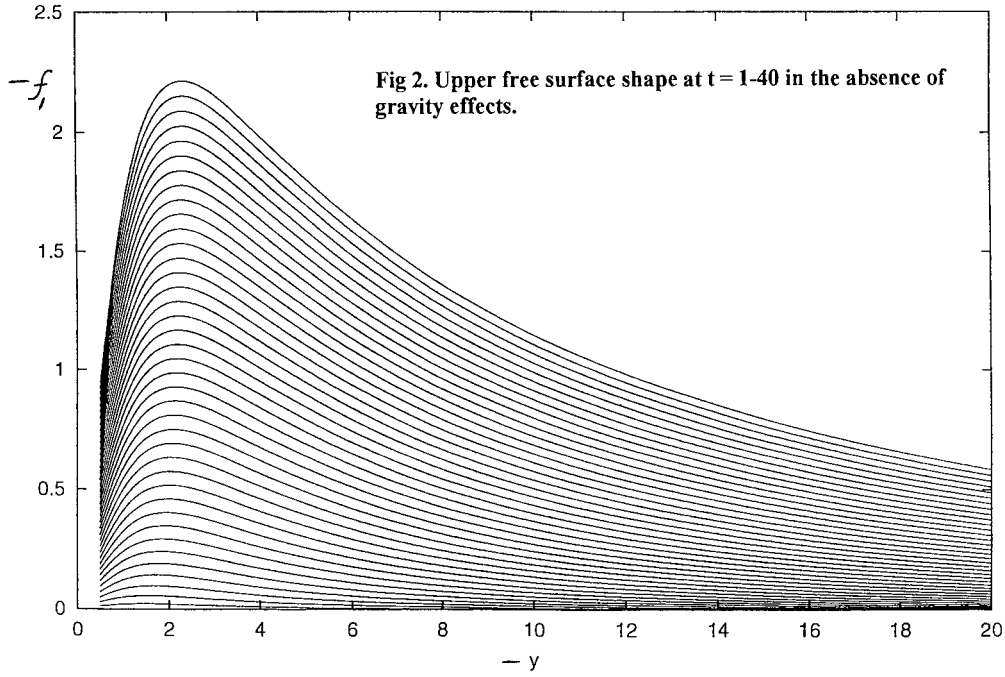

Figure 2. Upper free surface shape at $t = 1{-}40$ in the absence of gravity effects.

for the value of $\Psi_t = \psi_t^*$ along the upper and side edges of the inviscid region 3. Here $\bar{x}_A = -k^2$, the upper edge has $\bar{x} = y^2$ and the side edge has $\bar{x} = -x^2$, while $\delta_0(t)$ denotes the value of δ at the moving trailing edge which is the contact point. We recall that here u_w, k are 1, t, respectively. The two δ_0' terms in (3.5) cancel out for the side edge but not for the upper edge. The value (3.5) at $x = 0$ leads to the evolution of the scaled upper free surface f_1 as displayed in Figure 2. This is because the kinematic condition at the upper free surface $x = \mathrm{Re}^{-1/2} f_1(y, t) \ll 1$ is $u = \mathrm{Re}^{-1/2} f_{1t} + v\mathrm{Re}^{-1/2} f_{1y}$ in full but u, v are given by (3.1) and so the balance

$$u^* = f_{1t} \quad \text{at} \quad x = 0$$

is required. In consequence $\Psi_y = f_{1t}$, giving $\Psi_{yt} = f_{1tt}$. On the other hand, along $x = 0$ we have $y = -\bar{x}^{1/2}$, with $\bar{x}$ being positive and y being negative here. It follows that

$$f_{1tt} = -2\bar{x}^{1/2}\Psi_{\bar{x}t},$$

where the right-hand side can be determined from differentiating (3.5), for $\bar{x} > 0$. Thus f_{1tt} is determined. A double integration with respect to t gives f_1, which is shown in Figure 2 (in the results t increases from bottom to top), using results for $\delta(x, t)$ derived in the next section. The upper free surface is seen to rise monotonically with t and this is sensible physically in view of the positive and increasing viscous displacement by the descending plate and the absence of gravity effects: compare Section 5. Behaviour very similar to that in Figure 2 has been observed in direct simulations even at quite low Reynolds numbers and Froude numbers, for example in [2]'s results at $\mathrm{Re} = 20$, $Fr = 20$ for water free-surface motion near the descending side of a part-submerged rotating circular cylinder.

The scaled shape of the side free surface f_2 follows from the note at the end of the paragraph containing (2.3a,b) which shows that $-\Psi_x \to \delta_x - f_{2t}$ at the outer edge of the thin wake, since $\hat{V}(\equiv -\tilde{V}) \to \delta_x$ then. So on integration with respect to x the relations

$$f_{2t} = -\bar{f}_{2x}, \text{ with } \bar{f}_2(x,t) = -\Psi(x,0,t) - \delta_W(x,t), \tag{3.6}$$

determine f_2 for the range $0 < x < t$, where δ in the wake is written δ_W. It is interesting that both the inviscidly induced effect (3.5) with $\bar{x} = -x^2$ and the viscous wake displacement $\delta = \delta_W$ in (3.6) are involved in determining f_2. Results for the side free surface f_2 are presented in the next section.

At least four other small regions or thin layers are present in the water flow. These are: a small zone close to the leading edge at $x = k + 1$; small zones near the trailing edge at $x = k$; a small zone surrounding the intersection of the upper and side free surfaces near the origin; and a viscous layer along the upper free surface, in contrast with the wake layer region 2 along the side free surface. A description of these is presented in Appendix B.

4. Method, and results in the simplest case

Numerical solutions were obtained first for the simplest case above where gravity is negligible and no slip applies as in (2.4a): see Section 5 for the inclusion of gravity effects and slippage.

The numerical method for the unsteady boundary-layer and wake problem, a nonlinear evolution problem considered earlier by [15–17], consisted of the following. First, both equations are transformed into a fixed domain $(x, y) \in [0, 1] \times [0, +\infty)$, and then we put $\tilde{\eta} = y/2t^{1/2}$ and $\eta = 2/\pi \arctan \tilde{\eta}$ to account for the initial singularity in time and the variation across the boundary layer. The resulting equations are discretized with the θ-method in time and central differencing for both first and second derivatives in η. Here a conservative form of the convective term was employed, similar to the well-known Davis coupled scheme [18, pp. 218-221] for steady boundary layer problems. It was found that a method based on a nonconservative form of the convective terms works only for the wake, not the boundary layer. The ensuing discretized system is solved by marching downstream and at each station iterating for the continuity equation, which is discretized with a trapezoidal scheme. The resulting algorithm is very efficient and robust for both the boundary layer and wake. The numerical method for the scaled surface shape f_2 was based on either integrating along the characteristic lines and solving an ODE, or transforming to a fixed domain [0,1] and solving a PDE, the results from each approach agreeing closely. The integral in (3.5), which is involved in the calculation of f_2, needs special treatment. Direct calculation of the integral leads to

$$\partial_t(\bar{f}_2 + \delta_W) = \frac{(k^2(t) - x^2)^{1/2}}{\pi} \int_{-(k(t)+L)^2}^{-k^2(t)} \frac{\delta_t(\bar{\xi}, t)\, \mathrm{d}\bar{\xi}}{(-k^2(t) - \bar{\xi})^{1/2}(x^2 + \bar{\xi})}.$$

Then this integral has to be transformed into the corresponding interval in which the boundary-layer displacement δ is defined. That means that the actual effect of the boundary-layer displacement δ on f_2 comes from both time and space variation. A further transformation is also needed to eliminate the singularity in the integral. Finally the resulting integral is evaluated by a trapezoidal rule.

The whole computational procedure thus involved, at each time level, solving the unsteady boundary-layer equations and calculating δ; solving the unsteady wake equations by taking

the solution of the boundary layer at the trailing edge as upstream condition and calculating $\delta = \delta_W$; solving the equation for the side free surface, using the δ so obtained.

The main results are given in Figure 3(a,b). We observe the large range of t covered, and note that $\delta = 0$ at the original top level $x = 0$ as u reverts to 1 across the entire wake; any disturbances travel with free stream speed 1 at most in the downward moving frame. In addition δ exhibits the known irregularity $[\delta_0(t) - 0(\hat{x}_m^{1/3})]$ due to the Goldstein near-wake form in region 2 just above the trailing-edge contact point, the coordinate $\hat{x}_m = (t - x)$ being zero at that point. For small t the boundary layer and wake are given mostly by the Rayleigh form and a local similarity solution, respectively, whereas at large t the Blasius form holds on the plate, far below the top level, as is evident at $t = 10$. Just above the contact point ($f_2 = 0$)

$$f_2 \propto \hat{x}_m^{1/3} \tag{4.1}$$

with a positive coefficient of proportionality, due to the $-\hat{x}_m^{1/3}$ implicit in δ_W in (3.6): see Appendix B. Also, f_2 increases monotonically with t at each x station, which is again sensible physically because of the downward-plunging viscous displacement and indicates that there is no impingement of the side free surface on to the plate surface here (compare the gravity effect of the following section). Near the top, however, a wave-like response occurs which becomes almost stationary, at large t, and suggests that a small gravity effect could eventually lead to impingement: see next section.

5. Gravity and slip contributions

5.1. Froude-number effects

Concerning gravity, we consider the changes in the flow balances in regions 1–3 above as the inverse Froude number, $\mathrm{Fr}^{-1} \equiv \hat{g} = gL/U^2$, is increased gradually from zero, for instance as the downward-plunging velocity scale U is decreased. Since the inertial forces present are at their smallest, of order $\mathrm{Re}^{-1/2}$, in the outer region 3, it is clear that the effects of $\hat{g}$ are first felt within region 3 when $\hat{g}$ is still small, specifically when $\hat{g}$ becomes $\mathrm{Re}^{-1/2}\tilde{g}$ with $\tilde{g}$ of 0(1). There is still no effect at leading order then in the boundary-layer and wake regions 1 and 2, because there the inertial forces are typically of order unity. With the effects of gravity appearing in the outer region, the inviscid solution there (again see Appendix A) leads to

$$\partial_t(\bar{f}_2 + \delta_W) = -(k^2(t) - x^2)^{1/2}\left[\frac{1}{\pi}\int_{-(k(t)+L)^2}^{-k^2(t)} \frac{\delta_t(\bar{\xi}, t)\mathrm{d}\bar{\xi}}{(-k^2(t) - \bar{\xi})^{1/2}(x^2 + \bar{\xi})} + \tilde{g}\right], \tag{5.1}$$

which is the required extension of (3.5) (evaluated now along the side edge) and (3.6). Figure 3(c–f) gives some sample results. Figure 3(c,d) shows that relatively small gravity yields waves not unlike those for zero gravity but, in contrast with Section 4, here impingement occurs eventually in all cases. For any non-zero $\tilde{g}$ there is a bubble (impingement) formed above the contact point at some positive time denoted by t_{crit}, and moreover

$$t_{\mathrm{crit}} \sim \tilde{g}^{-2/3} \quad \text{for large } \tilde{g}. \tag{5.2}$$

This relation is discussed further in Section 6 and it holds in practice for $\tilde{g}$ above about 2 (see Figure 3g). The critical time is positive and finite for any positive $\tilde{g}$ because, on the one hand, the $+x_m^{1/3}$ behaviour of f_2 stays intact at the contact point throughout but, on the

other hand, $\bar{f}_{2x}$ responds as $x\tilde{g}\ln t$ at large times, from (5.1). This balance is reflected in the findings for various $\tilde{g}$ in Figure 3. Further, if $x = x_{\rm crit}$ is the location of touchdown where $f_2(x, t_{\rm crit}) = 0$, Figure 3(h) shows $x_{\rm crit}$ to be monotonically decreasing with $\tilde{g}$ which again is sensible physically.

5.2. SLIPPING EFFECTS

With slip effects, the contact point $x_c(t)$ slips relative to the plate and it forms a moving (decelerating) trailing edge. With initial length L normalised to unity again, the boundary layer is defined in $x \in [x_c, k+L]$ and a slip condition is imposed on the plate $Y = 0$; compare Appendix B. The wake region has δ, u continuous with the boundary-layer values at $x_c\pm$. These are the only alterations. After the Prandtl conversion as in Section 2, the boundary layer has

$$\hat{u}_{\hat{Y}} = \lambda\hat{u}, \quad \hat{V} = 0 \quad \text{at} \quad \hat{Y} = 0, \tag{5.3}$$

and $\hat{u} \to k'(t)$ as $\hat{Y} \to \infty$, while the wake has $0 < x \leqslant x_c(t)$. The equation for the side free surface is modified to (5.1) with right-hand side

$$-(x_c^2(t) - x^2)^{1/2}\left[\frac{1}{\pi}\int_{-(k(t)+L)^2}^{-x_c^2(t)} \frac{\delta_t(\bar{\xi}, t)\,\mathrm{d}\bar{\xi}}{(-x_c^2(t) - \bar{\xi})^{1/2}(x^2 + \bar{\xi})} + \tilde{g}\right]. \tag{5.4}$$

The determination of $x_c(t)$ can be achieved by solving the unsteady boundary-layer equations with varying length $\hat{L}(t) = k(t) + L - x_c(t)$. Obviously we have $\hat{u}(\hat{L}, 0, t) = L'(t) = k'(t) - x_c'(t)$, an implicit equation for $x_c(t)$, which was discretized by a backward Euler scheme. Therefore, iteratively solving the boundary-layer equations coupled with the above discretized equation determines x_c and so $\hat{L}$ at each time level. The whole computational procedure of iteration with slip accommodated is thus as before except for some details.

The slip conditions investigated are simple, namely (5.3) with

$$\text{[Slip condition 1]} \quad \lambda = 5, 1, 0.5; \tag{5.5a}$$

$$\text{[Slip condition 2]} \quad \lambda = c\left(\frac{1}{\hat{x}}\right)^r, \quad \hat{x} \in [0, \hat{L}(t)], \tag{5.5b}$$

where c, r are constants. See also Appendix B. Figure 4 shows the δ solutions up to $t = 4$ and, for 3 cases, f_2 with slip condition 1 applying for different λ values. The qualitative features are the same, although increased slip corresponding to decreased λ clearly reduces the size of δ and the length of the side free surface (wake), but the free surfaces keep almost the same shape for a given $\tilde{g}$. Figure 4 emphasises the effects on f_2 due to slip, through condition 1, as well as the influence of varying $\tilde{g}$. Properties at the impingement time $t_{\rm crit}$ are shown. Again there is virtually no qualitative difference, but the shrinking of the wake is evident both for an increased slip factor and for increased $\tilde{g}$. Figure 5(a–d) is for the slip condition 2, giving δ, f_2 for varying values of $\tilde{g}$, with $c = 1$ and $r = 1, 1{\cdot}5$. The overall effects are again interesting and coincide with those described earlier. Figure 5(e–g) continues the theme for the slip condition 2. Here $c = 1$ and $r = 2$, giving further enhanced slipping towards the trailing-edge contact point. Localised waves of a known kind can appear in δ and in the plate surface velocity after a finite time within the boundary layer, due to the increasing slip. They have no apparent strong influence on f_2, however, and they are eradicated at a

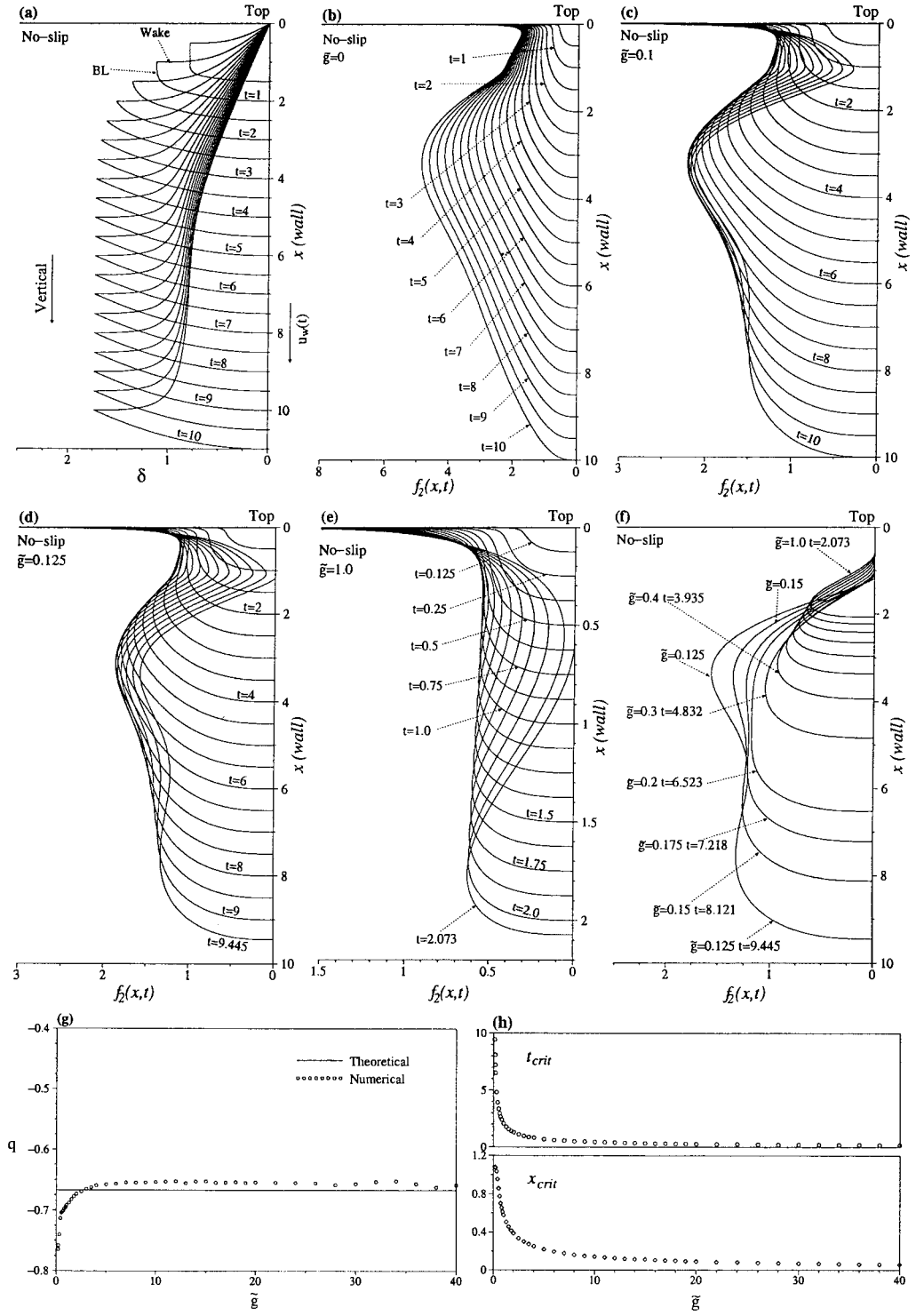

Figure 3. No-slip. (a) BL & Wake displacement thickness $\delta(x,t)$. (b) $f_2(x,t)$ for $\tilde{g} = 0$. (c) $f_2(x,t)$ for $\tilde{g} = 0{\cdot}1$. (d) $f_2(x,t)$ for $\tilde{g} = 0{\cdot}125$. $f_2(x_{\text{crit}}, t_{\text{crit}}) = 0$ with $x_{\text{crit}} = 1{\cdot}183$ and $t_{\text{crit}} = 9{\cdot}445$. (e) $f_2(x,t)$ for $\tilde{g} = 1{\cdot}0$. $f_2(x_{\text{crit}}, t_{\text{crit}}) = 0$ with $x_{\text{crit}} = 0{\cdot}578$ and $t_{\text{crit}} = 2{\cdot}073$. (f) $f_2(x, t_{\text{crit}})$ for different $\tilde{g} = 0{\cdot}125, 0{\cdot}15, 0{\cdot}175, 0{\cdot}2, 0{\cdot}3, \ldots, 0{\cdot}9, 1{\cdot}0$, *i.e.*, the shapes at the time bubbles are implied. (g) Plot of $q = \Delta \ln(t_{\text{crit}})/(\Delta \ln(\tilde{g}))$ against $\tilde{g}$. (h) Plots of t_{crit} and x_{crit}) against $\tilde{g}$.

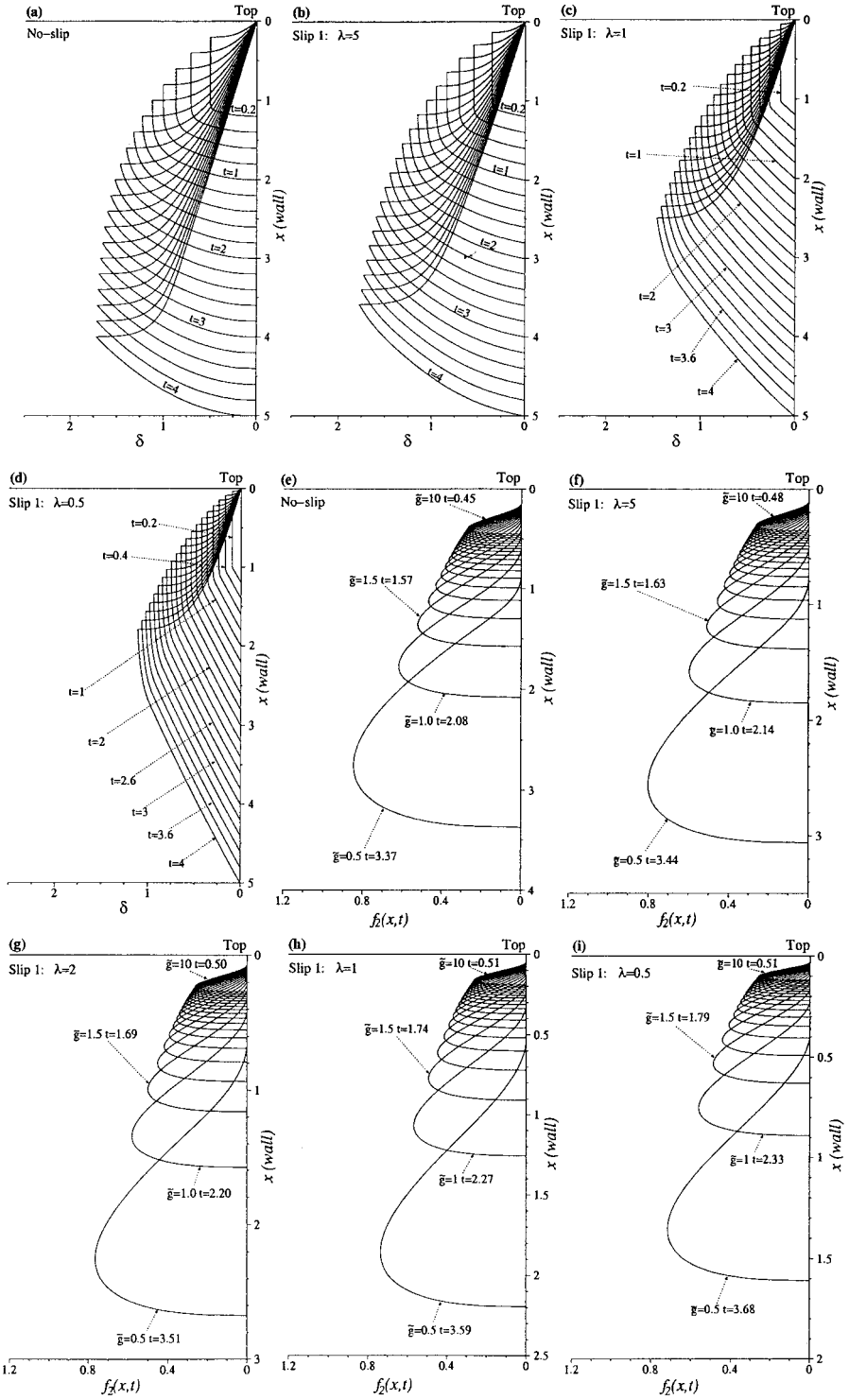

Figure 4. Slip condition 1. (a–d) Displacement $\delta(x, t)$ for no-slip and slip condition 1. (e–i) Shapes of side free surface $f_2(x, t), t = t_{\text{crit}}$ with $\tilde{g} = 0{\cdot}5, 1, 1{\cdot}5, 2, \ldots, 9, 9{\cdot}5, 10$ for no-slip and slip condition 1.

smaller c value; Figure 5(h,i) presents f_2 for the case of $c = 0{\cdot}5, r = 2$. Finally Figure 6 plots the location of the contact point x_c versus t for various λ values in condition 1 and for various c, r values in condition 2. The last two point to the emergence of a similarity response as t increases, in which u scales with 1 and hence x_c with t. Likewise x, y, v scale with $t, t^{1/2}, t^{-1/2}$, respectively. This response remains to be followed through.

6. Further comments

It is of immediate interest that the gravity effect first appears via $\tilde{g}$ in the inviscid outer region 3, not via $\hat{g}(= \mathrm{Fr}^{-1})$ in the nonlinear inner regions. This gravity effect $\tilde{g}$ forces the side free surface to impinge on the plate within a finite time, suggesting bubble formation subsequently. Indeed the extra effect $\propto \tilde{g}$ if considered on its own causes the upper free surface to fall ($u^* > 0$ there) and the side surface to impinge immediately on the plate above the contact point (since $v^* > 0$ then), as one would expect of enhanced gravity. This leads not only to the impingement trends seen in the earlier figures as $\tilde{g}$ increases but also to the result (5.2), and Figure 3(d), when combined with the overriding influence of the viscous displacement just above the contact point. Slip conditions by contrast have no qualitative influence on the free-surface shapes prior to a bubble forming, although the shapes do shrink with increasing slip.

The result (5.2) that the critical time scales with $\tilde{g}^{-2/3}$, when $\tilde{g}$ is large, shows that the dimensional time t_D involved is independent of the original submerged length L, due to the L/U and $\mathrm{Re}^{-1/2}U^2/L$ factors implicit in $t, \tilde{g}$, respectively. This independence also makes good physical sense, since the critical wake lengths as well as times are so short then. The dimensional time t_D is also found to be independent of the dimensional downward speed U then, because the inherent viscous Rayleigh thickness $(\nu t_D)^{1/2}$ yields an acceleration $\nu^{1/2}t_D^{-3/2}$ which is comparable with that of gravity g when $t_D \sim g^{-2/3}\nu^{1/3}$. It is observed also that there is no significant stress singularity over the length scales considered in this study.

Other geometric shapes of body yield a similar flow structure, even if the body thickness is of 0(1), in which case u, v, ψ, p in the bulk of the water motion become of order unity instead of being as in (3.1). Downward plunging thin body shapes other than the flat plate were mentioned near the end of Section 2 and can be accommodated readily in the analysis, by virtue of the Prandtl transposition property. Thus δ is simply replaced by $\delta + f_3$, where $f_3(x, t)$ denotes the $\mathrm{Re}^{-1/2}$ scaled moving body thickness in the horizontal direction.

Subsequent points of interest are these. First, calculations with slip conditions should continue and be made more realistic. Second, treating a single or a few closed air bubbles is difficult but may actually simplify for many bubbles. The overall viscous region then is relatively thick (and long) compared with each individual bubble, according to an analogy with the multiple boundary layer-and-wake setting in [19]. That leaves the overall, outer, viscous region as one subject to a quasi-no-slip constraint at the solid surface, as in Section 4, whereas each (small) bubble is immersed in uniform shear flow. Attempts may continue nevertheless for the case of few bubbles. Third, direct Navier-Stokes simulations, *e.g.* as in [2, 20], and experiments would be useful for comparison, and work by us on the former is in progress. Fourth, the upward-moving plate partially submerged at time zero poses another fundamental problem of concern, and likewise for an oscillating plate and for a rotating partially submerged circular cylinder. Finally, the air flow has been assumed to be dynamically negligible, at least until the verge of impingement. This assumption needs checking, as follows, especially in the

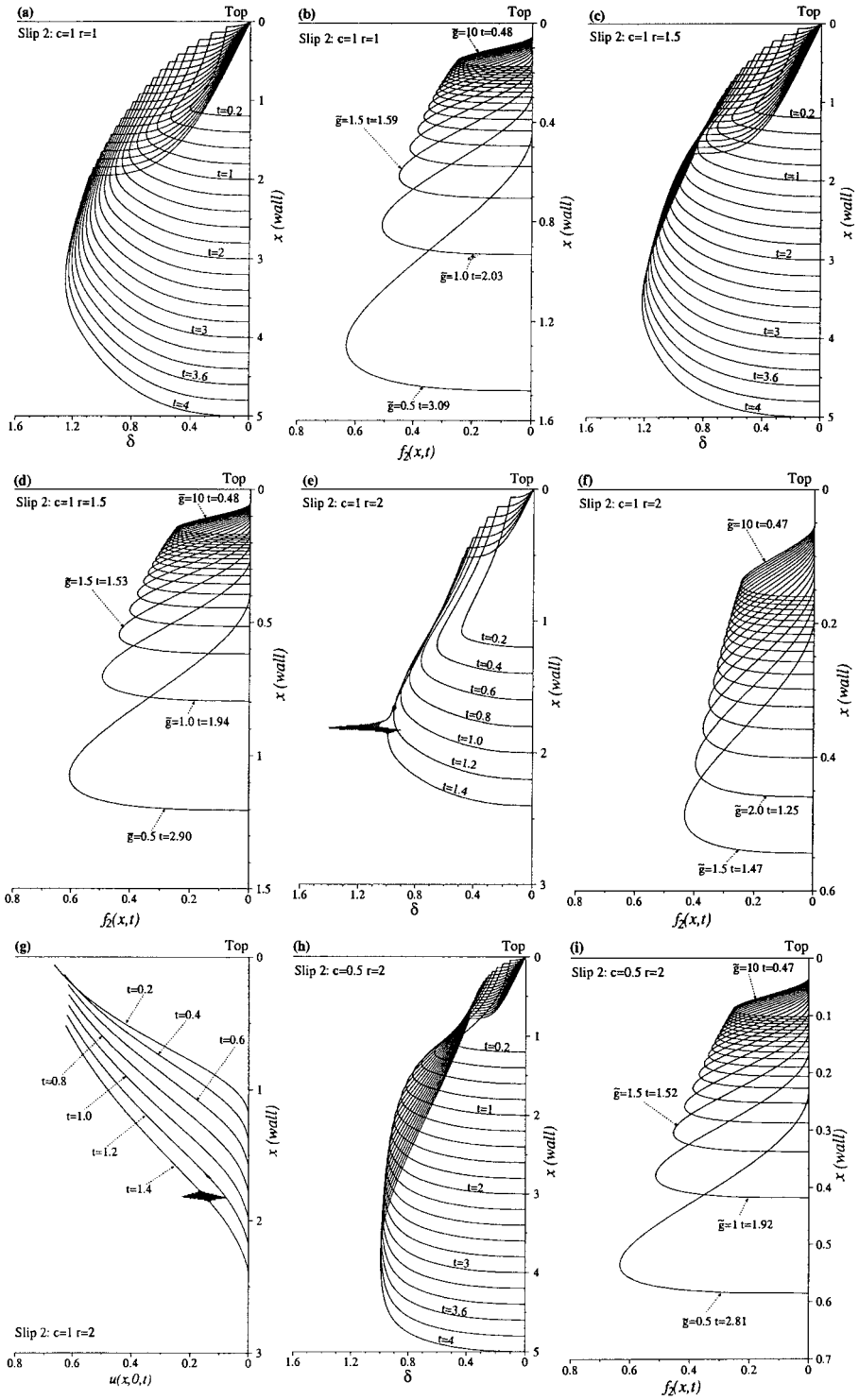

Figure 5. Slip condition 2. (a,c,e,h) Displacement $\delta(x, t)$. (b,d,f,i) Shapes of side free surface $f_2(x, t)$, $t = t_{\text{crit}}$ for $\tilde{g} = \cdot 5, 1{\cdot}0, 1{\cdot}5, 2{\cdot}0, \ldots, 9{\cdot}0, 9{\cdot}5, 10$. (g) Velocity on the plate for $c = 1$, $r = 2$. The numerical solution breaks down at $t = 1{\cdot}5363$.

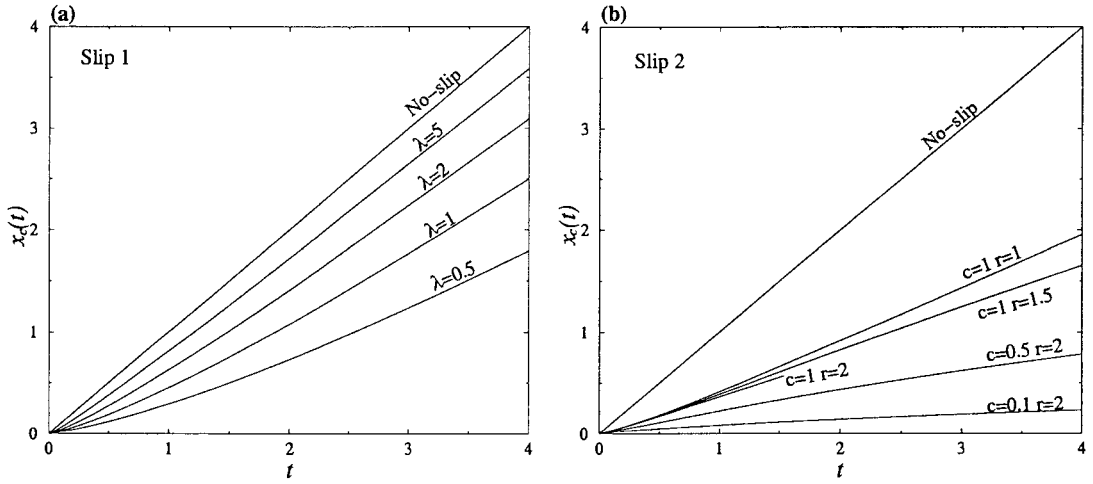

Figure 6. Plot of $x_c(t)$ against t for (a) slip condition 1 and (b) slip condition 2.

air gap between the side free surface and the plate above its trailing-edge contact point since that gap is thin. There, due to the kinematic viscosity of air being only about 16 times that of water, the representative air boundary-layer thickness is approximately only 4 times that of water and so can be taken to be the same, of order $\mathrm{Re}^{-1/2}$. Hence the air pressure gradients generated are of a characteristic size equal to the density ratio ρ_{air}/ρ, given the continuity at the air-water interface of u which is 0(1) in the water wake. These extra pressure gradients are thus negligible compared with those generated in the bulk of the water flow as given in (3.1) with x, y of order one provided that $\rho_{\mathrm{air}}/\rho \ll \mathrm{Re}^{-1/2}$. In consequence the requirement

$$\mathrm{Re} \ll (\rho/\rho_{\mathrm{air}})^2 \tag{6.1}$$

holds on the theory in the present paper. The right-hand side here is about 10^6, for example for dry air and pure water at one-atmosphere pressure, and so Re can still be reasonably large while satisfying (6.1). Impingement, during which air-water interaction does enter play, is studied by [21].

Acknowledgement

Financial support for L.L. and for computing from the Leverhulme Trust is gratefully acknowledged.

Appendix A. Solving in the inviscid region 3

This concerns the solution of (3.3) for the scaled pressure in the quarter-plane $x > 0$, $y < 0$ subject to (3.4a–e). From (3.2a–c) $p^* - \mathrm{i}\psi_t^*$ is an analytic function of $z = x + \mathrm{i}y$ since $u^* = \partial\psi^*/\partial y$, $v^* = -\partial\psi^*/\partial x$.

A transformation to a half-plane ($\mathrm{Im}\bar{z} > 0$) is afforded by the mapping

$$\bar{z} = -z^2, \tag{A1}$$

where $\bar{z} = \bar{x} + \mathrm{i}\bar{y}$, say, giving $\bar{x} = y^2 - x^2$, $\bar{y} = -2xy$. Here the top edge $x = 0$, $y < 0$ is mapped to the positive real axis $\bar{x} = y^2$, $\bar{y} = 0$, while the side edge $y = 0$, $x > 0$ is mapped

to the negative real axis $\bar{x} = -x^2$, $\bar{y} = 0$. In particular, the transformed trailing-edge position is at $\bar{x} = -t^2$ ($\equiv \bar{x}_A$ say) and the leading edge is at $\bar{x} = -(t+1)^2 (\equiv x_C$ say) for the main case $u_e = 1$, $k = t$.

The function $p^* - i\psi_t^*$ is analytic in $\bar{z}$ in the upper half-plane $\bar{y} > 0$ and satisfies mixed boundary conditions along the x-axis, from (3.4a,c–e),

$$p^* = 0 \quad \text{at} \quad \bar{y} = 0, \quad \bar{x} > \bar{x}_A, \tag{A2}$$

$$p^*_{\bar{y}} = \bar{h}(\bar{x}, t), \quad \bar{y} = 0, \bar{x} < \bar{x}_A, \tag{A3}$$

as well as the condition of zero p^* in the far field. In (A3), $\bar{h}$ which is $\partial^2\psi^*/\partial\bar{x}\partial t(\bar{x}, 0)$ from the Cauchy-Riemann equations is equal to $-\partial^2\delta/\partial\bar{x}\partial t$, *i.e.* $(2x)^{-1}\partial^2\delta/\partial x\partial t$ [see (3.4d)] for the interval $\bar{x}_C < \bar{x} < \bar{x}_A$ corresponding to the plate and $\bar{h}$ is zero for $\bar{x} < \bar{x}_C$ corresponding to the symmetry condition (3.4e).

The function $(\bar{z} - \bar{x}_A)^{-1/2}[p^* - \mathrm{i}\psi_t^* - \mathrm{i}\delta_0'(t)]$ is likewise analytic, with the δ_0' making this function finite at $\bar{z} = \bar{x}_A$, while the inverse square root is defined as $|\bar{z} - \bar{x}_A|^{-1/2}\exp(-\mathrm{i}\bar{\theta}/2)$ with $\bar{\theta} \equiv \tan^{-1}(\bar{y}/(\bar{x} - \bar{x}_A))$ being zero along $\bar{y} = 0$ for $\bar{x} > \bar{x}_A$ and π along $\bar{y} = 0$ for $\bar{x} < \bar{x}_A$. Hence the real part of the function is prescribed all along the $\bar{x}$-axis, from (A2),(A3). Its imaginary part therefore follows directly from the Cauchy-Hilbert integral of the known real part. That yields the equation

$$-(\bar{x} - \bar{x}_A)^{-1/2}(\psi_t^* + \delta_0') = -\frac{1}{\pi}\int_{-\infty}^{\bar{x}_A}(\bar{x}_A - \bar{\xi})^{-1/2}(\delta_0' - \delta_t(\bar{\xi}, t))\frac{\mathrm{d}\bar{\xi}}{(\bar{x} - \bar{\xi})} \tag{A4}$$

along the real axis of $\bar{z}$, for $\bar{x} > \bar{x}_A$, associated in the z-plane either with the top edge or with the side edge above the contact point. In obtaining (A4) the condition $\psi^* = -\delta$ (at $\bar{y} = 0$, $\bar{x} < \bar{x}_A$) has again been used.

The relation (A4) gives the result (3.5) quoted in the text. The lower bound of integration in (3.5), (A4) is kept as $-\infty$ because although $\delta_t(\bar{\xi}, t)$ is identically zero for $\bar{\xi} < \bar{x}_C$ the term $\delta_0'(t)$ is nonzero.

Including gravity yields the explicit form

$$\tilde{g}x - \tilde{g}\left\{z + (z+t)^{1/2}(z-t)^{1/2}\right\}, \tag{A5}$$

to be added to $p^* - \mathrm{i}\psi_t^*$ in the z plane. The term $\tilde{g}x$ (in p^*) balances the gravity force in the x-momentum equation. Here and above the appearance of square roots is as expected, given the mixed boundary conditions. The branches of the square root functions in (A5) are defined such that $(z+t)^{1/2}$ is $|z+t|^{1/2}\exp(\mathrm{i}\theta_1/2)$ with $\theta_1 \equiv \tan^{-1}(y/(x+t))$ and θ_1 being between 0 and π in the region $y < 0$, and similarly for the other square root with argument $\theta_2/2$. All the required boundary conditions are satisfied by (A5). In particular at large distances within the water $p^* \sim \tilde{g}x$, $u^* \to 0$, $v^* \to 0$ (since $\psi^* \to 0$), to leave vanishing flow there, while at the upper surface the properties $x = 0$, $z = \mathrm{i}y$, $(\theta_1 + \theta_2)/2 = \pi/2$ throughout imply that $p^* = 0$ there, matching the atmospheric pressure; at higher order (3.4a) would include a contribution $p^* = -\tilde{g}f_1\mathrm{Re}^{-1/2}$ but this is negligible here as $\tilde{g}$ is $O(1)$. Likewise, along the side surface $y = 0$, above the trailing-edge contact point we have $z = x$ and $(\theta_1 + \theta_2)/2$ remains $\pi/2$, so that p^* remains at atmospheric zero, whereas below the trailing edge $(\theta_1 + \theta_2)/2$ is π which gives the additional ψ_t^* being zero and thus keeps the δ-effect on the total ψ^* unaltered. The extra contribution to ψ_t^* concerned with the side free surface is $\tilde{g}(t^2 - x^2)^{1/2}$ from (A5) and therefore produces the explicit form given in (5.1) when used with (3.6).

Appendix B. Other regions, at order-one times

For the leading-edge and contact regions we work in a coordinate frame moving with the plate, similarly to Section 2, so that

$$(x, y, u, v, \psi, p) = (1 + t - \hat{x}, -\hat{y}, 1 - \hat{u}, -\hat{v}, \hat{\psi}, \hat{p}). \tag{B1}$$

The unsteady Navier-Stokes equations in usual form then apply to $\hat{u}, \hat{v}, \hat{\psi}, \hat{p}$ in coordinates $\hat{x}, \hat{y}, t$, subject to no slip on the plate $\hat{y} = 0$ for $0 \leqslant \hat{x} \leqslant 1$, standard free-surface conditions for $\hat{x} > 1$, symmetry conditions at $\hat{y} = 0$ for $\hat{x} < 0$ and $\hat{u} = 1$, $\hat{v} = \hat{p} = 0$ sufficiently far from the plate.

The small leading-edge region then has the well-known scalings of $\hat{x} \sim \hat{y} \sim \mathrm{Re}^{-1}$, $\hat{u} \sim \hat{v} \sim \hat{p} \sim 1$, $\hat{\psi} \sim \mathrm{Re}^{-1}$, which leave the steady Navier–Stokes equations holding in full with Re replaced by unity in effect. The solution satisfying the symmetry, no-slip and matching conditions is as in [22].

Near the contact point (trailing edge), $\hat{x} \to 1$, we start by re-considering the unsteady boundary layer 1 and wake 2. The first relation in (3.6) becomes $\partial \bar{f}_2/\partial \hat{x} = \partial f_2/\partial t + \partial f_2/\partial \hat{x}$ in the moving system and thus implies that locally $\partial \bar{f}_2/\partial \hat{x} \sim \partial f_2/\partial \hat{x}$ for t of order one. The requirement $\partial \delta_W/\partial \hat{x} + \partial \bar{f}_2/\partial \hat{x} = 0$ locally also from (3.6) coupled with the local behaviour

$$\delta = \delta_W \sim \delta_0(t) - (\hat{x} - 1)^{1/3}\delta_1(t) \tag{B2}$$

therefore gives the side-free-surface shape as

$$f_2 \sim (\hat{x} - 1)^{1/3}\delta_1(t) \tag{B3}$$

for $\hat{x} \to 1+$ (downstream). Here $\delta_1(t)$ is positive and of order unity for $t \sim 1$. The requirement above is in order to satisfy the zero-pressure constraint at order $\mathrm{Re}^{-1/2}$ on the free surface. Upstream $\delta \sim \delta_0(t) + 0(1 - \hat{x})$ due to layer 1, as $\hat{x} \to 1-$. The mismatch with (B2) has to be smoothed out through shorter length scales close to $\hat{x} = 1$. One might expect the quasi-steady triple-deck structure to provide this smoothing via the length scaling $\hat{x} - 1 = \mathrm{Re}^{-3/8}X$ with $|X| \sim 1$, as in totally immersed trailing-edge flows [23, Chapters 23–25], but that appears not to be the case here. Instead the results (B2),(B3) continue to apply throughout the $\mathrm{Re}^{-3/8}$ region, with the combination of negative viscous displacement variation (B2) and positive free-surface displacement (B3) yielding zero total variation in displacement effectively: in traditional triple-deck notation the present solution has

$$P \equiv 0, A \equiv 0, \tag{B4}$$

where $p = \mathrm{Re}^{-1/4}P$ and $-A$ is the scaled total variation in displacement, while the lower-deck flow has uniform shear flow for all $X < 0$ and the viscous Goldstein near-wake form (Prandtl-shifted by the free surface at zero pressure P) for all $X > 0$. The quasi-steady water flow streamlines, outside the local viscous layers, thus remain more parallel to the plate here, compared with the immersed case. The final smoothing actually occurs in a smaller zone where $|\hat{x} \sim 1|$, $\hat{y}$ are both of order $\mathrm{Re}^{-3/4}$, $\hat{u} \sim \hat{v} \sim \mathrm{Re}^{-1/4}$, $\hat{p} \sim \mathrm{Re}^{-1/2}$ and so the quasi-steady Navier-Stokes equations again hold in full with Re replaced by unity. This is as in [22, 24, 25] but the boundary conditions are different here in that the unknown free surface is present and the matching condition is new downstream. There the Goldstein near-wake solution applies in terms of the shifted 0(1) similarity coordinate

$$\eta = \frac{\mathrm{Re}^{3/4}\hat{y} - [\mathrm{Re}^{3/4}(\hat{x}-1)]^{1/3}\delta_1}{[\mathrm{Re}^{3/4}(\hat{x}-1)]^{1/3}} \tag{B5}$$

for $\hat{y} \gg \mathrm{Re}^{-1/2}(\hat{x}-1)^{1/3}\delta_1$. The edge $\eta = 0$ where $\partial\hat{u}/\partial\hat{y}$ vanishes corresponds to the free surface, matching with (B3), maintaining the zero pressure condition and giving zero total displacement variation outside the viscous layer. The flow details at the contact point including slippage can also be considered to lie within the small $0(\mathrm{Re}^{-3/4})$ zone as opposed to those studied in Section 5.2.

The top corner, which is the origin in terms of x, y, is where the side free surface and upper free surface must merge. The scaled motion there is again controlled by the full Navier-Stokes equations since locally x, y scale with $\mathrm{Re}^{-1/2}$ and u, v with $\mathrm{Re}^{-1/2}$, so that inertial and viscous farces are both $0(\mathrm{Re}^{-1/2})$, with the pressure response being $0(\mathrm{Re}^{-1})$. Unlike in the other regions above, the motion here is unsteady however, for $t \sim 1$. Thus, with the full free-surface constraints also holding, and matching with the other regions incorporated, a challenging problem is set for the top-corner dynamics.

Finally, viscous effects close to the upper free surface must allow the constraints of zero tangential stress to be satisfied there. Since (3.2b,c) shows inertial forces to be negligible in region 3 nearby, the main viscous operator $\mathrm{Re}^{-1}\partial^2/\partial x^2$ has only to balance the temporal operator $\partial/\partial t$ within the free-surface layer. The viscous scaling is therefore $|x| \sim \mathrm{Re}^{-1/2}$ and the known, linear, viscous unsteady problem near a free surface is obtained.

References

1. P.R. Garabedian, Oblique water entry of a wedge. *Comm. Pure Appl. Math.* 6 (1953) 157–165.
2. J.F. Thompson, Numerical solution of flow problems using body-fitted coordinate systems. In: W. Kollman (ed.), *Computational Fluid Dynamics*. Washington (D.C.): Hemisphere Pub. Corp. (1980) 1–98.
3. M. Greenhow, Wedge entry into initially calm water. *Appl. Ocean Res.* 9 (1987) 214–223.
4. D.G. Dommermuth, D.K.P. Yue, W.M. Lin, R.J. Rapp, E.S. Chan and W.K. Melville, Deep-water plunging breakers: a comparison between potential theory and experiments. *J. Fluid Mech.* 189 (1988) 423–442.
5. S.D. Howison, J.R. Ockendon and S.K. Wilson, Incompressible water-entry problems at small deadrise angles. *J. Fluid Mech.* 222 (1991) 215–230.
6. M.J. Cooker, Recent numerical calculations of two-dimensional jets induced by breaking-wave impact; a comment. *Phil. Trans. R. Soc.* A355 (1997) 687–689.
7. M.J. Cooker, Violently erupting free-surface jets. In: A.C. King and Y.D. Shikmurzaev (eds.), *Free-Surface Flows*. Proc. IUTAM Symp., Birmingham, U.K. (2001) pp. 63–70.
8. M.J. Cooker, P.D. Weidman and D.S. Bale, Reflection of a high-amplitude solitary wave at a vertical wall. *J. Fluid Mech.* 342 (1997) 141–158.
9. S. Somalinga and A. Bose, Numerical investigation of boundary conditions for moving contact line problems. *Phys. Fluids* 12 (2000) 499–510.
10. R.G. Cox, The dynamics of the spreading of liquids on a solid surface. Part 1. Viscous Flow. *J. Fluid Mech.* 168 (1986) 169–194.
11. R.G. Cox, The dynamics of the spreading of liquids on a solid surface. Part 2. Surfactants. *J. Fluid Mech.* 168 (1986) 195–200.
12. R.G. Cox, Inertial and viscous effects in dynamic contact angles. *J. Fluid Mech.* 357 (1998) 249–278.
13. K. Stoev, E. Ramé and S. Garoff, Effects of inertia on the hydrodynamics near moving contact lines. *Phys. Fluids* 11 (1999) 3209–3216.
14. C. Härtel, E. Meiburg and F. Necker, Analysis and direct numerical simulation of the flow at a gravity-current head. Part 1. Flow topology and front speed for slip and no-slip boundaries. *J. Fluid Mech.* 418 (2000) 189–212.
15. M.G. Hall, The boundary layer over an impulsively started flat plate. *Proc. R. Soc. London* A310 (1969) 401–414.

16. D.P. Papadopoloulos, On the unsteady boundary layer and wake of a flat plate, and modelling water flow near a ship-side. Ph.D. thesis, Univ. of London (2000) 248. pp.
17. L. Li, D.P. Papadopoulos, F.T. Smith and G.-X. Wu, Water flow due to rapid part-submerged body movement. Proc. IUTAM Symp. on Free-Surface Flows, Birmingham, UK, July 2000. Kluwer pubs. (2001) 177–185.
18. C.A.J. Fletcher, *Computational Techniques for Fluid Dynamics, vol. II* (1991).
19. F.T. Smith and S.N. Timoshin, Planar flows past thin multi-blade configurations. *J. Fluid Mech.* 324 (1996) 355–377.
20. M. Sussman, P. Smereka and S. Osher, A level set approach for computing solutions to incompressible two-phase flow. *J. Comp. Phys.* 114 (1994) 146–159.
21. F.T. Smith, L. Li and G.-X. Wu, Air cushioning with a lubrication/inviscid balance. Submitted to *J. Fluid Mech.* (2001).
22. A.E.P. Veldman and A.I. van de Vooren, Drag of a finite flat plate. In: R.D. Richtmeyer (ed.): *Lecture Notes in Physics* 35. Berlin: Springer-Verlag (1976) 422–430.
23. A.P. Rothmayer and F.T. Smith, *Incompressible Triple Deck Theory*. CRC *Handbook of Fluid Dynamics* (1998) 823 pp.
24. K. Stewartson, On the flow near the trailing edge of a flat plate II. *Mathematika* 16 (1969) 106–121.
25. F.T. Smith, R.G.A. Bowles and L. Li, Nonlinear effects in absolute and convective instabilities of a near-wake. *Eur. J. Mech.* B19 (2000) 173–211.